Asian Journal of Pharmaceutical Sciences 19 (2024) 100889

Available online at www.sciencedirect.com

ScienceDirect

journal homepage: www.elsevier.com/locate/AJPS

Research Article

MSC-derived exosomes attenuate hepatic fibrosis in primary sclerosing cholangitis through inhibition of Th17 differentiation

Wenyi Chen[a], *Feiyan Lin*[a], *Xudong Feng*[a], *Qigu Yao*[a], *Yingduo Yu*[a], *Feiqiong Gao*[a], *Jiahang Zhou*[a], *Qiaoling Pan*[a], *Jian Wu*[a], *Jinfeng Yang*[a], *Jiong Yu*[a], *Hongcui Cao*[a,c,*], *Lanjuan Li*[a,b]

[a] *State Key Laboratory for the Diagnosis and Treatment of Infectious Diseases, National Clinical Research Center for Infectious Diseases, Collaborative Innovation Center for Diagnosis and Treatment of Infectious Diseases, National Medical Center for Infectious Diseases, The First Affiliated Hospital, Zhejiang University School of Medicine, Hangzhou 310003, China*

[b] *Jinan Microecological Biomedicine Shandong Laboratory, Jinan 250117, China*

[c] *Key Laboratory of Diagnosis and Treatment of Aging and Physic-chemical Injury Diseases of Zhejiang Province, Hangzhou 310003, China*

ARTICLE INFO

Article history:
Received 13 July 2023
Revised 13 December 2023
Accepted 14 January 2024
Available online 12 February 2024

Keywords:
Mesenchymal stem cell
Exosomes
Primary sclerosing cholangitis
Fibrosis
Organoids
Th17

ABSTRACT

Primary sclerosing cholangitis (PSC) is an autoimmune cholangiopathy characterized by chronic inflammation of the biliary epithelium and periductal fibrosis, with no curative treatment available, and liver transplantation is inevitable for end-stage patients. Human placental mesenchymal stem cell (hpMSC)-derived exosomes have demonstrated the ability to prevent fibrosis, inhibit collagen production and possess immunomodulatory properties in autoimmune liver disease. Here, we prepared hpMSC-derived exosomes (Exo^{MSC}) and further investigated the anti-fibrotic effects and detailed mechanism on PSC based on $Mdr2^{-/-}$ mice and multicellular organoids established from PSC patients. The results showed that Exo^{MSC} ameliorated liver fibrosis in $Mdr2^{-/-}$ mice with significant collagen reduction in the preductal area where Th17 differentiation was inhibited as demonstrated by RNAseq analysis, and the percentage of $CD4^{+}IL\text{-}17A^{+}T$ cells was reduced both in Exo^{MSC}-treated $Mdr2^{-/-}$ mice ($Mdr2^{-/-}$-Exo) in vivo and Exo^{MSC}-treated Th17 differentiation progressed in vitro. Furthermore, Exo^{MSC} improved the hypersecretory phenotype and intercellular interactions in the hepatic Th17 microenvironment by regulating PERK/CHOP signaling as supported by multicellular organoids. Thus, our data demonstrate the anti-fibrosis effect of Exo^{MSC} in PSC disease by inhibiting Th17 differentiation, and ameliorating the Th17-induced microenvironment, indicating the promising potential therapeutic role of Exo^{MSC} in liver fibrosis of PSC or Th17-related diseases.

* Corresponding author.
E-mail address: hccao@zju.edu.cn (H. Cao).
Peer review under responsibility of Shenyang Pharmaceutical University.

https://doi.org/10.1016/j.ajps.2024.100889

1. Introduction

Primary sclerosing cholangitis (PSC) refers to cholangiopathies characterized by progressive fibro-obliteration of the intra- and/or extra-hepatic bile ducts, associated with chronic inflammation of the biliary epithelium and periductal "onion-skinning-like" fibrosis [1–3]. As an autoimmune cholestatic liver disease, cholangiocytes in PSC patients are likely targeted by T cell-driven immune attack, leading to cholestasis, ductopenia, and, finally, end-stage liver disease [4,5]. Genetic and environmental factors such as microbiological effects combined with dysregulated adaptive and innate immune responses also contribute to the progression of PSC [4,6–8], but the detailed pathophysiology mechanisms remain unknown [5]. There are no curative treatments yet, and liver transplantation is needed for end-stage patients [9,10].

Research on PSC is moving slowly and is limited by the difficulty in accessing the cholangiocytes, the instability of in vitro culture systems, and the reliance on samples from the end-stage disease [10]. Therefore, alternative research models are required for further study. Mouse models, such as disruption of the tight junctions of cholangiocytes [3,11,12] or failure of biliary phospholipid secretion [13], have been established. Multidrug resistance gene 2 knockout ($Mdr2^{-/-}$ or $Abcb4^{-/-}$) mice is a genetic model that resembles PSC in patients who lack the canalicular phospholipid flippase, leading to a potential increase in toxic bile acid and causing hepatocyte damage and cholangiopathy [11,14,15], followed by the development of peri-cholangitis and onion skin-type periductal fibrosis, resembling the pathological features of PSC [16,17].

Moreover, cultures of hepatic cells, such as biliary epithelial cells with stimulators to mimic pathogenic bile duct cells, are regarded as in vitro classical research models. However, classic two-dimensional monolayer cell cultures do not resemble the interaction and communications between cells. Organoids, a new three-dimensional (3D) cell culture system, have been developed in recent years, the cells of which recapitulate the native physiology of original tissue-derived cells [18], such as bile duct cells, and resemble the cellular interaction, microenvironment, cellular function, and architecture of hepatic cells in vivo [18–20], holding greater potential to become experimental models for liver diseases [5]. Furthermore, with the explosive development, organoids containing multiple cell types, which we herein call composite organoids or multicellular organoids, have been developed and applied in preclinical disease modeling [21,22], tumor microenvironment researching [23], drug screening [24], and studies of pathogenic mechanisms [25,26]. However, organoids developed from liver-derived stem cells have limitations, as they contain either cholangiocytes or hepatocytes, unlike the composite organoids including multiple cell types produced from other organs, such as lungs and intestines. Here, we innovatively developed multicellular-organoids formed by 3D co-culture of hepatocytes or hepatic stellate cells with cholangiocytes to mimic the intrahepatic microenvironment of PSC.

In PSC livers, although the main cholangiopathies are bile duct disorders, impairment of the bile epithelium as initiated by functional changes (cellular senescence and genetic mutations) or by biliary insults (bile acid toxicity, microbial factors, and inflammatory mediators) remains unclear [10]. Continuous inflammatory insults on cholangiocytes result in a reactive inflammatory phenotype of cholangiocytes: highly secreting proinflammatory and profibrotic chemokines or cytokines, the hypersecretory phenotype tightly connected to the ductular reaction and liver fibrosis [27–30]. Shreds of evidence show that the chemokines/cytokines secreted by cholangiocytes, especially chemokine (C–C motif) ligand 20 (CCL20), can attract T helper 17 (Th17) lymphocytes to damage bile ducts in liver diseases [31]. But few treatments were found to regulate cytokines secretion or differentiation of Th17 [32,33]. Nevertheless, the secretion of interleukin-17A (IL-17A) from Th17 cells directly activates hepatic stellate cells (HSCs) [34,35], and the levels of circulating IL-17A are associated with the development of mice liver fibrosis [34]. Moreover, IL-17A signaling, found in recent experimental clinical observations, is related to the fibrogenesis of the lungs, skin, and livers [36,37]. On the other hand, incubation of cholangiocytes with IL-17A leads to an immune-reactive phenotype with the high secretion of proinflammatory mediators, including CCL20 [10], which indicates a positive feedback pathway between cholangiocytes and Th17 cells.

However, during the progression of liver fibrosis, cholangiocytes themselves do not express collagen type-I (Col1) [13]; other hepatic cells, including HSCs, hepatocytes, and macrophages, are involved in the pathophysiology of inflammatory responses and fibro-genic activities [5,38]. As one of the three major collagen type-I-producing myofibroblast original cells (HSC, portal fibroblast, and fibrocyte) [39–42], HSCs show a tight connection with cholangiocytes [43]. Researchers have verified that signals secreted by cholangiocytes cause paracrine responses in HSCs, which leads to liver fibrosis during injury [30,38]. For instance, transforming growth factor β1(TGF-β1) stimulation changed quiescent HSCs (qHSCs) into $Col1^{+}aSMA^{+}$ myofibroblasts (aHSCs) [39], which is critical for alpha-smooth muscle actin (α-SMA) expression and extracellular matrix protein (mostly Col1) accumulation [44]. In addition, the trans-differentiation between hepatocytes and cholangiocytes during biliary damage/severe hepatocyte loss also indicates the importance of the crosstalk between cholangiocytes and hepatocytes [45].

Human mesenchymal stem cells (MSCs) possess immunomodulatory properties, such as inhibition of the proliferation of T cells through the programmed death-1 (PD-1) pathway [46–48], influencing the release of Th17 cytokines (IL-17A and IL-22) [49]. They also have the capacity to inhibit cytokine production [50], which indicates their potential in therapy for liver fibrosis dominated by bile duct pathology. As the endosomal origin of MSCs with a diameter size ranging from 40 to 160 nm [51], exosomes not only have the advantages of being cell-free, noninvasive, less immunogenic, and nontoxic [52], but more importantly, they are well tolerated during repeated injections in patients [53].

Researchers recently found that MSC-derived exosomes can repair liver function [54] and ameliorate liver fibrosis [55] by inhibiting collagen production [56–58] and repairing the hepatic fibrosis and inflammatory markers of autoimmune liver disease [59]. Furthermore, mediating the micro-molecule transfer to HSCs and regulating the collagen maturation gene expression [60,61] helps to alleviate hepatic fibrosis [62]. In addition, our previous researches demonstrated the anti-senescence effect of human placental MSCs (hpMSCs) or hpMSCs derived exosomes (Exo^{MSC}) towards senescent cholangiocytes (cholangiocytes organoids), one of the typical pathological features of PSC, reducing the senescent-associated-type (SASP) components (IL-6, CCL2, CXCL1, etc.) and cell cycle arrest proteins (p21 and p16) [63,64].

Some studies have demonstrated the therapy of MSCs on liver fibrosis-related diseases and the mechanisms involved [65,66], but the role of the paracrine effect of MSCs on the hepatic portal microenvironment in PSC disease has not been investigated before. Here, we used the $Mdr2^{-/-}$ mice as in vivo model and PSC patient-derived organoids combined with liver parenchymal cells to construct composite organoids as in vitro models to explore the more detailed mechanism of Exo^{MSC} on PSC.

2. Materials and methods

2.1. Materials

2.1.1. Protein-producing cells and animals

Stably transfected 293T cells producing Rspon1-Fc fusion protein for culturing organoids was obtained as a gift from Professor Enkui Duan at the Chinese Academy of Sciences. $FVB.Mdr2^{+/+}$ (Wild type, WT) and $FVB.Mdr2^{-/-}$ mice were obtained from The Jackson Laboratory (Bar Harbor, Maine, USA). The mice were bred and maintained under specific pathogen-free conditions at the Ziyuan Animal Base (Hangzhou, China) and subjected to experiments at the animal center of The First Affiliated Hospital, Zhejiang University School of Medicine. Male mice were used in the experiments presented. All animal experiments were approved by the Animal Experimental Ethical Inspection of the hospital (reference No. 2020-1088).

2.1.2. Cell lines and maintenance

Human HSCs (LX2) and human hepatocytes (LO2) were cultured in Dulbecco's modified Eagle's medium (DMEM, Gibco, US) [high glucose, with GlutaMAX and pyruvate, 10% fetal bovine serum (FBS, Gibco), and 1% penicillin/streptomycin (Corning, US)]. LX2 cell line was obtained from Shanghai Biotechnology Company (Shanghai, China), while LO2 cell line was provided by our laboratory. Human liver tissue, peripheral blood mononuclear cells (PBMCs), and placenta were obtained from donors at the First Affiliated Hospital, Zhejiang University School of Medicine. All protocols for human tissue and cell handling were approved by the Clinical Research Ethics Committee of the hospital (reference No. 2013–272, 2021–158).

2.2. Intrahepatic cholangiocytes isolation and culture of organoids

Biliary epithelial cells were isolated in our laboratory according to established protocols [67]. Briefly, the liver tissue (0.5–1.0 mm^3) was washed with washing medium (DMEM containing GlutaMAX and pyruvate with 1% FBS, 1% penicillin, and streptomycin), and then digested in 4–5 ml pre-warmed 37 °C digestion medium [DMEM containing 0.1 mg/ml DNase I (Sigma-Aldrich, USA), 2.5 mg/ml of collagenase D (Roche, Switzerland), and Dispase II (Life Technologies, USA)] shaking for 0.5–1.5 h. After washing and centrifugation, the cell precipitate was collected.

Cholangiocytes (8×10^4) were resuspended in 50 µl Matrigel (Corning, USA) per well (24-well plates) (Corning) and covered with 500 µl expansion medium (Ad DMEM/F-12 (Gibco, USA) supplemented with 1:50 B27 supplement (Life Technologies, USA), 1:100 N2 supplement (Life Technologies, USA), 1 mM N-acetylcysteine (Sigma-Aldrich, USA), 5% (v/v) Rspon1-conditioned medium, 10 mM nicotinamide (Sigma-Aldrich, USA), 10 nM (Leu15)-gastrin I (Sigma-Aldrich, USA), 50 ng/ml of epidermal growth factor (EGF, Life Technologies, US), 100 ng/ml of fibroblast growth factor 10 (FGF10, PeproTech, USA), 25 ng/ml of hepatocyte growth factor (HGF, PeproTech, USA), 10 µM of forskolin (Tocris Bioscience, UK), and 5 Mm A83–01(Tocris Bioscience, UK) after the solidification of Matrigel. The expansion medium was changed every 2-3 d. The passaging procedure was performed after 7–14 d of culture. Detailed procedures of the cryopreservation and recovery were described elsewhere [63,67].

2.3. Organoid modeling and exosome administration

After the organoids (Passage1–5) were stably cultured for 2 d, 100 ng/ml of IL-17A (PeproTech, USA) was added to the expansion medium as suggested previously [68]. Meanwhile, 10 ng/ml Exo^{MSC} was used to verify the function in the microenvironment produced by IL-17A. Cultures and cultural supernatant were collected and analyzed after 3 d of treatment, respectively. The procedure for acquiring Exo^{MSC} has been provided in the supplementary material.

2.4. Trans-well culture of organoids and HSCs/hepatocytes

Cholangiocytes (5×10^4) digested from cholangiocyte-organoids (Orgs) were seeded in 30 µl of Matrigel in the upper chamber and cultured with 300 µl expansion medium; simultaneously, 1×10^5 HSCs or hepatocytes were seeded in the 24-well plate and cultured with DMEM (containing 10% FBS and 1% penicillin/streptomycin). After culturing individually for 1 d, the medium in the upper chamber was replaced with fresh expansion medium, and the medium of the hepatocytes or HSCs was replaced with 200 µl fresh DMEM medium (without FBS), and the upper chamber was inserted into the hepatocytes- or HSCs-containing well. Then 100 ng/ml IL-17A and 10 ng/ml Exo^{MSC} were added accordingly. After 3 d, the cultures in the upper and lower chambers were collected and analyzed.

2.5. Establishment of the HSC-Orgs/hepatocyte-Orgs co-culture 3D model

The Orgs were digested, and single cholangiocytes were prepared as described before [67]. Single cells of HSCs/hepatocytes were prepared by resuspending them in DMEM (without FBS). Next, cholangiocytes at 5×10^4 cells per well and HSCs/hepatocytes at 8×10^4 cells per well (24-well plates) were mixed and subsequently centrifuged at 350 g and 4 °C for 5 min to remove the supernatant. The pellets were collected and embedded in Matrigel with an appropriate volume of 50 µl per well in 24-well plates. After the Matrigel solidified, the mixtures were covered with 500 µl expansion medium, which was subsequently replaced every 2 to 3 d.

To establish the IL-17A-induced 3D co-culture model, we replaced the expansion medium with fresh expansion medium containing 100 ng/ml IL-17A after 2 d of co-culture, together with 10 ng/ml Exo^{MSC} as appropriate. Subsequently, we conducted analyses using immunofluorescence (IF) staining and immunohistochemical (IHC) staining analyses after an additional 3 d of cultivation. The morphology was recorded through light microscopy.

2.6. Membrane staining with PKH67

The PKH67 Green Fluorescent Cell Linker Kit (Sigma-Aldrich, USA) was used following the manufacturer's instructions.

Staining of Orgs: A suitable quantity of Orgs (5–7 d) was collected and digested into single cells using TrypLE solution (Gibco, USA), as described previously [67]. The cells were washed once with PBS 1 × and resuspended in 1 ml Diluent C to prepare a 2 × cell suspension. Then, the 2 × dye solution (4×10^{-6} M) was prepared by adding 1 ml diluent C to 4 µl PKH67. Next, the 2 × cell suspension was rapidly mixed with the 2 × dye solution and allowed to settle for 1–5 min with several overblows; the staining was stopped by adding 1 ml FBS or 1% (w/v) bovine serum albumin (BSA) solution and incubated for 1 min. After centrifugation and three times washing, cells were re-embedded into Matrigel for Orgs culture as described before.

Staining of Exo^{MSC}: The extracted exosomes were added to 1 ml of Diluent C, mixed with the prepared 2 × dye solution, and incubated in the dark for 4 min. After stopping the incubation, Exo^{MSC} were washed once with PBS 1 × and ultracentrifuged at 110,000 × *g* 4 °C for 1 h. Finally, the PKH67-labelled exosomes were collected and resuspended with an appropriate volume of PBS 1 × .

2.7. Immunostaining analysis

Organoids were completely harvested using Cell Recovery Solution (Corning, USA). (1) IHC staining: organoids were washed once with PBS 1 ×, dehydrated in 70% ethanol (Sango Biotech, China), and stained in 0.5% eosin (Sango Biotech, China; dissolved in 96% ethanol) for 30 min. After rehydration in 100% ethanol, the organoids were embedded in paraffin. The subsequent procedures were the same as the normal IHC steps. The data were analyzed using ImageJ (https://imagej.net/Download) (2) IF staining: after fixation with 4% (w/v) paraformaldehyde (Absin, China) at 4 °C, the organoids were washed in 0.1% (v/v) Tween-PBS (Sango Biotech, China) and blocked with TritonX-100-BSA solution. Primary antibodies were used to incubate the organoids in 24-well plates at 4 °C overnight. After one wash, the organoids were incubated with corresponding secondary antibodies, before finally being transferred to slides with coverslips and observed under laser scanning confocal fluorescence microscopy (LSCFM) (Leica, FV3000). The detailed procedures were described previously [63,67].

Immunostaining of mouse liver tissue slides for markers, including cytokeratin 19 (CK19/Krt19), albumin (Alb), α-SMA, and IL-17A, was performed using a Novo-Light Multiplex Fluorescence Immunohistochemical Kit (WiSee Bio, China). The complete list of immunostaining antibodies used can be found in Table S1.

2.8. Statistical analyses and reproducibility

The data are presented as the mean ± SD and represent a minimum of three independent experiments. The FVB male mice ($Mdr2^{-/-}$/$Mdr2^{+/+}$) were randomly assigned to groups. Statistical significance for each experiment was determined as shown in the figure legends. Statistical analyses were performed in GraphPad Prism 8.0.1 (GraphPad Software Inc., La Jolla, USA), and statistical significance was evaluated with two-tailed unpaired Student's *t*-tests or one-way ANOVAs accordingly. The data were assigned as not significant (ns); $^*P < 0.05$; $^{**}P < 0.01$; $^{***}P < 0.001$. All images are representative of at least three independent experiments.

3. Results and discussion

3.1. $Mdr2^{-/-}$ mouse-based tracking of PSC hepatic fibrosis progression

To reveal the progress of fibrosis and degree of liver function impairment during disease progression before Exo^{MSC} injection, 7- to 13-week-old $Mdr2^{-/-}$ mice and WT ($Mdr2^{+/+}$) mice were sacrificed, and their livers were collected for further analysis. Meanwhile, serum was obtained to verify the levels of alanine aminotransferase (ALT), aspartate aminotransferase (AST), and alkaline phosphatase (ALP). The results showed that liver fibrosis became more severe with increasing weeks of $Mdr2^{-/-}$ mice (Fig. S1A), and onion skin-like pathology in the hepatic confluence area presented after eight or nine weeks of age, as well as measured by Masson staining (Fig. S1B) and Sirius Red staining (Fig. S1C), while collagenous fibers were stained blue in Masson and red in Sirius Red staining. In addition, ALT, AST and ALP levels showed a rising trend with age (Fig. S1D), indicating progressively severe damage of liver function.

3.2. hpMSC-derived exosomes alleviated liver fibrosis in $Mdr2^{-/-}$ mouse

To verify the hypothesis that Exo^{MSC} may exert therapeutic effects on $Mdr2^{-/-}$ mice, the exosomes were isolated

from the supernatant of hpMSCs by ultrahigh-speed centrifugation, and the integrity of the vesicles was confirmed by transmission electron microscopy (TEM) (Fig. S2A). Then, the mean main peak of three exosome samples was determined to be 116.97 nm (percentage of main peaks all >95%) via nanoparticle tracking analysis (NTA), and the average concentration of Exo^{MSC} was 1.47 × 10^{10} particles/ml for every 200 ml hpMSC-supernatant (Fig. S2B). The conventional exosome markers CD9, CD63, and Hsp70 were confirmed through western blot (WB) analysis (Fig. S2C). After this, eight-week-old Mdr2$^{-/-}$ mice were injected with 10.29 ± 2.81 μg (100 μl of ~6.75 × 10^8 particles/ml) of Exo^{MSC} or vehicle (100 μl PBS), as depicted in Fig. 1A. At weekly intervals, 3–5 mice were sacrificed to collect liver tissue, and their blood was collected via the inferior vena cava in blood collection tubes containing procoagulant, centrifuged at 2500 rpm for 15 min at room temperature, and serum collected and frozen at −80 °C for further analysis.

After Mdr2$^{-/-}$ mice received one injection of Exo^{MSC} (Mdr2$^{-/-}$-Exo), serum levels of ALT, AST, and ALP tended to increase, and then began to decrease gradually after the second injection. One week after the third injection, the serological indicators above decreased to a level like that of the Mdr2$^{-/-}$ mice, and one week after the fourth injection, all the above indexes were below that of Mdr2$^{-/-}$ mice, suggesting that Exo^{MSC} might cause a drastic response in a damaged liver during the pre-treatment period, but had no effect on normal livers (Mdr2$^{+/+}$-Exo). After four weeks of treatment, the serum levels of ALT, AST, and ALP decreased relative to Mdr2$^{-/-}$ mice group (Fig. 1B). Therefore, the 12-week time point was chosen as the endpoint of Exo^{MSC} therapy. Hence, α-SMA (Fig. 1C, D) and Sirius Red staining (Fig. 1E, F) were performed and quantified on 12-week-old mice, and the results proved that the α-SMA and collagen levels were reduced significantly by Exo^{MSC} treatment. Furthermore, Desmin (an active marker of HSCs) and glial fibrillary acidic protein (GFAP, an early activation marker of HSCs) exhibited reduced expression in the portal area of Exo^{MSC}-treated Mdr2$^{-/-}$ mouse liver, as shown in Fig. 1G-1J. Moreover, the highly expressed level of the fibrosis-relevant genes (*Tnf-α*, *Tgf-β1*, *Tgf-β2*, *Acta2*, *Col3a1* and *Cola1*) in Mdr2$^{-/-}$ mice were down-regulated significantly by Exo^{MSC} therapy, especially *Tnf-α*, *Tgf-β1*, *Tgf-β2* and *Acta2* (Fig. 1K), indicating the anti-fibrotic effect of Exo^{MSC}.

3.3. Exo^{MSC} treatment influenced the differentiation of Th17 in vivo

To further clarify the mechanism by which Exo^{MSC} exerts the therapeutic effect, the liver RNA of Mdr2$^{+/+}$ mice, Mdr2$^{-/-}$ mice, and Exo^{MSC}-treated Mdr2$^{-/-}$ mice (Mdr2$^{-/-}$-Exo) were collected for RNA-Seq analyses. Differentially expressed gene data (Fig. 2A) showed the up- and downregulated gene numbers in comparison to the different groups. A total of 1172 genes were upregulated, while 315 genes were downregulated when comparing WT and Mdr2$^{-/-}$ mice. Exo^{MSC} might play a role in downregulating genes from a general perspective, in which 74 genes were downregulated when comparing Mdr2$^{-/-}$ and Mdr2$^{-/-}$-Exo mice. One intriguing observation from the gene set enrichment analysis (GSEA) results (Fig. 2B) was that functional differential gene expression of Th17 cell differentiation was down-regulated by Exo^{MSC} (NES -1.5823, false discovery rate 0.1236).

Further, Kyoto Encyclopedia of Genes and Genomes (KEGG) analysis of the gene set in Th17 cell differentiation (enrichment plot: KO04659) showed that these genes were also associated with pathways such as Th1 and Th2 cell differentiation, inflammatory bowel disease (IBD) genes, and programmed cell death ligand 1 (PD-L1) expression and the PD-1 checkpoint pathway in cancer (Fig. 2C). To verify whether Th17 in mouse livers was affected by Exo^{MSC}, the cell distribution and proportion of Th17 in the livers of the mice were analyzed via IHC staining and flow cytometry. We found that IL-17A staining of positive cells was mostly located near the hepatic confluent areas, and the livers of Mdr2$^{-/-}$ mice had significantly more IL-17A staining of positive cells than WT mice (Mdr2$^{+/+}$) (Fig. 2D), which is consistent with the typical intrahepatic IL-17A$^+$ T cell percentage data from the liver of PSC patient, as shown in Fig. S3, but reduced significantly in Exo^{MSC}-treated mice, as proven by flow cytometry (Mdr2$^{-/-}$ vs. Mdr2$^{-/-}$-Exo, $P = 0.028$) (Fig. 2E, F). Furthermore, the *Il-17a* gene expression of liver-infiltrating immune cells (WT vs. Mdr2$^{-/-}$, $P = 0.007$; Mdr2$^{-/-}$ vs. Mdr2$^{-/-}$-Exo, $P = 0.0264$) was also significantly decreased (Fig. 2G), implying a significant reduction in the cell percentages and gene expression content of Th17 in Mdr2$^{-/-}$ livers after exosome treatment, which might be due to the inhibition of Th17 differentiation by Exo^{MSC}.

3.4. Exo^{MSC} could inhibit Th17 differentiation in vitro

To further clarify the precise impact of exosomes on Th17, naïve CD4$^+$ T cells were collected from PBMCs of healthy donors by magnetic sorting, and then raised in Th17 differentiation medium for 13 d. Exosomes in different concentrations were added at 3-d intervals. Consequently, flow cytometry showed that percentages of CD4$^+$ IL-17A$^+$ T cells were significantly reduced by exosomes treatment (Fig. 3A, B), but the exosome concentration between 2~15 ng/ml showed no obvious difference in the IL-17A expression. During culture, the exosomes were engulfed intracellularly by T cells (Fig. 3C), and after 13 d, gene expression and cytokine level of IL-17A in Th17 cultures were significantly reduced by Exo^{MSC} treatment (Fig. 3D, E). These results suggest that Exo^{MSC} play a role in inhibiting Th17 differentiation and reducing IL-17A expression.

3.5. Exo^{MSC} moderated Th17-induced fibrosis-associated microenvironment in PSC

The evidence indicates that Exo^{MSC} reduced the hepatic fibrosis of Mdr2$^{-/-}$ mice and inhibited the differentiation of Th17 cells; however, whether Th17 is associated with hepatic fibrosis has not yet been clarified. Considering the lack of secretion of the collagen of cholangiocytes during hepatic fibrosis and the tight connection of cholangiocytes between HSCs and hepatocytes, we aimed to investigate the more elaborate microenvironment changes involved in PSC livers.

First, to construct a model that more closely replicates the in vivo liver environment, we established 3D Orgs

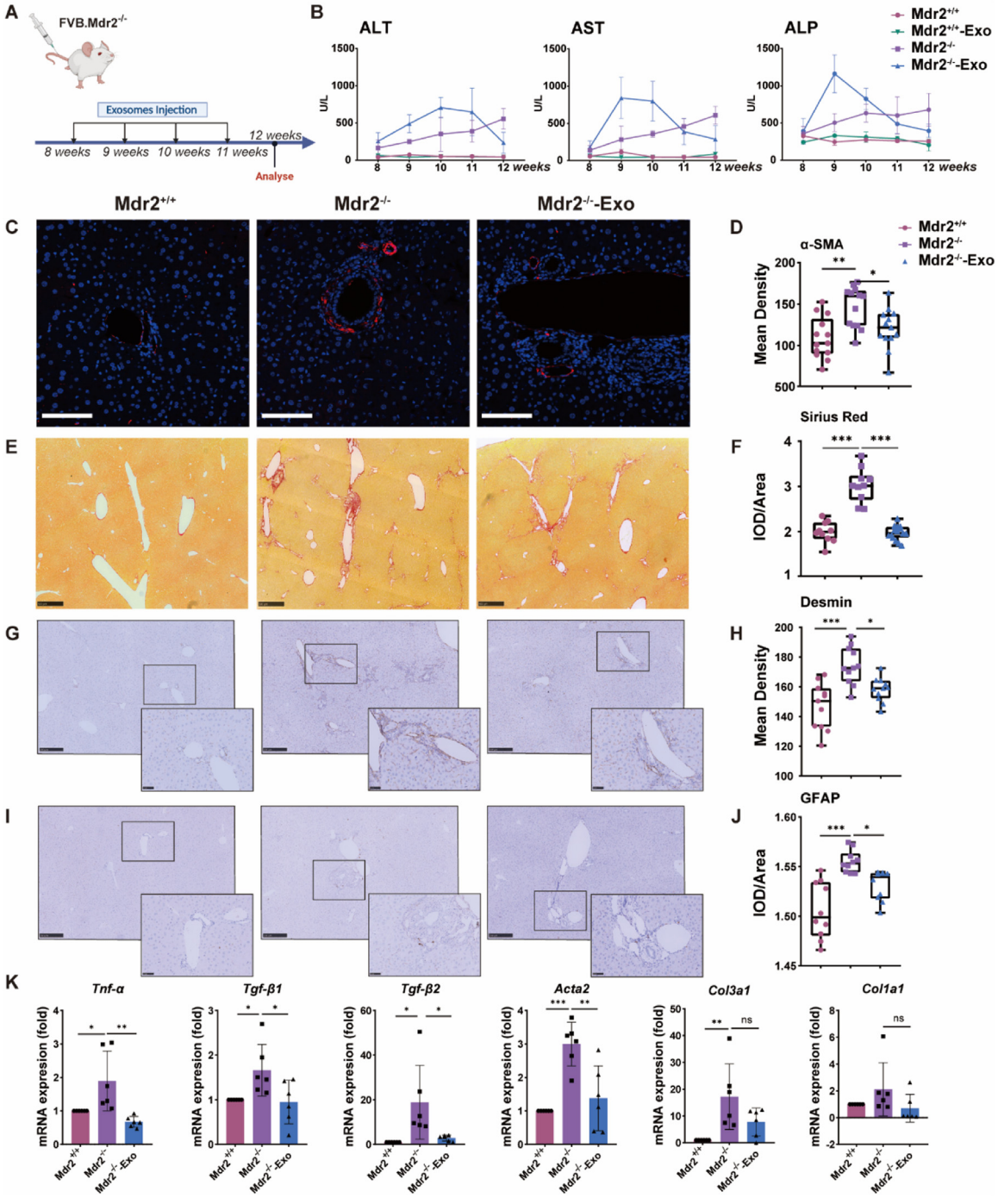

Fig. 1 – Exo^{MSC} alleviated liver fibrosis in Mdr2$^{-/-}$ mice. (A) Pattern-plot of the duration of Exo^{MSC} treatment in Mdr2$^{-/-}$ mice. Mdr2$^{+/+}$ (WT) mice, as the control group, were injected with counterpart PBS. (B) Mouse serum ALT, AST, and ALP levels after treatment. Mdr2$^{-/-}$ mice and Mdr2$^{+/+}$ mice treated with Exo^{MSC} as Mdr2$^{-/-}$-Exo and Mdr2$^{+/+}$-Exo, respectively (n = 3, mean ± SD). (C) IF assay of α-SMA (Red) from 12-week-old mice liver slides. (scale bar = 50 μm). (D) Semiquantitative analysis of α-SMA fluorescence staining results using ImageJ. Thirteen fields were randomly selected . (E) Semi-quantitative analysis of Sirius Red staining using ImageJ. A total of 10~15 views were randomly selected. (F) Sirius Red staining of 12-week-old mice (scale bar = 500 μm). (G) IHC taining of Desmin from 12-week-old mice liver (scale bar = 250 μm or 50 μm). (H) A total of 11 fields of Desmin IHC staining results were randomly selected and analyzed by ImageJ-Pro Plus. (I) Representative picture of GFAP IHC staining results (scale bar = 250 μm or 50 μm). (J) Ten fields of GFAP IHC staining were randomly selected and analyzed by ImageJ-Pro Plus. (K) Fold change in mRNA expression of the hepatic fibrosis-related genes in 12-week-old mice (n = 6, mean ± SD). *P < 0.05, **P < 0.01, ***P < 0.001.

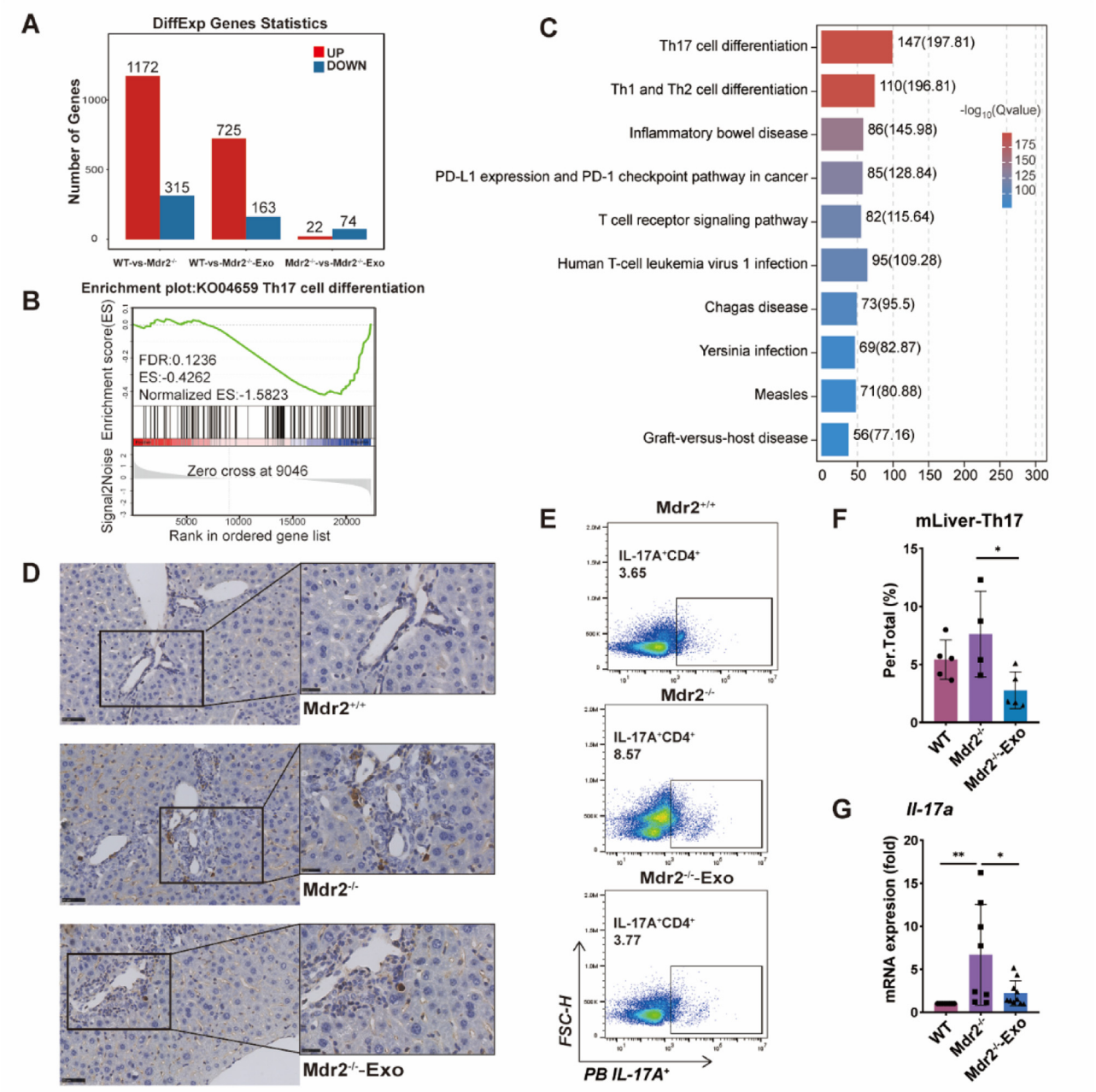

Fig. 2 – Exo^{MSC} treatment delayed Th17 differentiation in vivo. (A) Mouse liver RNA-seq data of the differentially expressed genes of Mdr2$^{+/+}$ mice, Mdr2$^{-/-}$ mice, and Mdr2$^{-/-}$-Exo mice. (B) GSEA results of Th17 cell differentiation. (C) KEGG analysis of the genes clustered in Th17 cell differentiation enrichment plot. Top 10 pathways were listed. (D) IL-17A IHC staining analysis of the mouse liver tissue sections. (scale bar = 50 μm (left column), scale bar = 25 μm (right column)). (E) Flow cytometry analysis of the intrahepatic immune cells in mouse liver. IL-17A$^+$ CD4$^+$ T cells were gated. (F) The percentages of IL-17A$^+$ CD4$^+$ T were counted and analyzed by FlowJo V10 (n = 4–5, mean ± SD,). (G) Fold change in mRNA expression of *Il-17a* gene expression by mouse intrahepatic immune cells (n = 8–10, mean ± SD).

from intrahepatic bile duct cells of PSC patients; the operation flow is shown in Fig. 4A. Additionally, the Orgs were identified as a 3D spherical structure composed of Krt19 expression cholangiocytes with functional transporting activities (Rhodamine 123, red), possessing normal cell cycle states such as proliferation (Ki67, red), senescence (P21$^{Cip1/Waf1}$, green), and apoptosis (Caspase-9/Cas-9, red) (Fig. 4B). To confirm the effect of IL-17A secreted by Th17 on Orgs, 100 ng/ml of IL-17A with or without exosomes was added to the expansion medium of Orgs, with the expansion medium alone as control group (Ctrl). The results show supernatant containing higher levels of the cytokines of C-X-

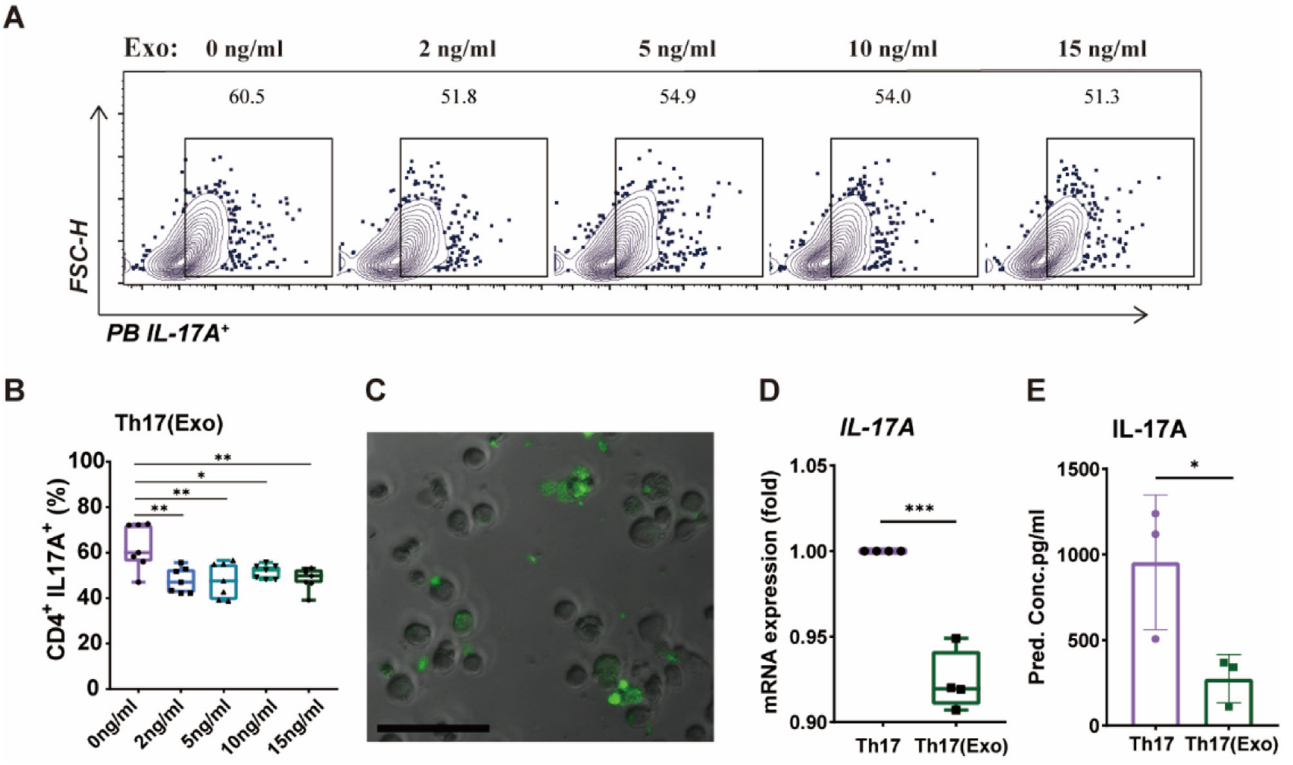

Fig. 3 – Exo^{MSC} inhibited Th17 differentiation in vitro. (A) Concentrations of 0, 2, 5, 10, and 15 ng/ml of Exo^{MSC} were added to the differentiation medium at 3-d intervals. IL-17A^{+}CD4^{+} T cells were assessed by flow cytometry, and (B) analyzed by FlowJo V10 ($n = 7$). (C) PKH-67-stained Exo^{MSC} (green) were internalized into Th17 cells during differentiation (scale bar = 20 μm). D. 2 ng/ml Exo^{MSC} were added at 3-d intervals during Th17 differentiation, and *IL-17A* gene levels of Th17 cells ($n = 4$, unpaired *t*-test) and (E) IL-17A cytokine levels in the supernatant were determined by ELISA at Day 13 ($n = 3$, unpaired *t*-test). *P < 0.05, **P < 0.01, ***P < 0.001).

C motif chemokine ligand 10 (CXCL10) and IL-6, as stimulated by IL-17A after 48 h. However, their expression was reduced due to the presence of exosomes (Fig. 4C).

To verify the hypothesis that Th17 is associated with liver fibrosis, as the main collagen fiber-producing cells in liver fibrosis, the human HSC cell line LX2 was used and cultured along with the simulation of 50 ng/ml of IL-17A. Results show that *collagen type I alpha 1* (*COL1A1*) and *collagen type III α1* (*COL3A1*) expression was elevated by IL-17A and significantly downregulated by the addition of Exo^{MSC} (Fig. 4D), indicating that fibrosis-related genes are highly related to IL-17A secreted by Th17. Furthermore, the chemotaxis assay shows that the supernatant of IL-17A and Exo^{MSC}-treated HSCs attracted fewer Th17 cells at 12 h compared to the supernatant of IL-17A-treated HSCs (Fig. 4E), indicating the essential role of HSCs in Th17 chemotaxis. However, the counterpart of hepatocytes presented a similar but milder tendency than the HSCs (Fig. 4F).

In conclusion, IL-17A secreted by Th17 could induce hypersecretory phenotype of cholangiocytes and upregulated fibrosis-associated genes of HSCs, which could be ameliorated by Exo^{MSC}. Exo^{MSC} also reduced Th17 chemotaxis to HSCs in the IL-17A-induced microenvironment.

3.6. Exo^{MSC} regulated HSC-cholangiocyte interaction to moderate Th17-induced fibrosis-associated microenvironment

We then further investigated whether cholangiocytes would influence HSCs and inhibit collagen accumulation and whether Exo^{MSC} would influence the interaction between HSCs and Orgs when they are stimulated by IL-17A. The PKH-67-stained Orgs (top chamber) and HSCs (bottom chamber) were cultured together in a trans-well chamber (Orgs-H) (Fig. 5A). After IL-17A treatment, HSCs showed stronger green fluorescence signals in response to IL-17A, indicating enhanced secretion of PKH67-stained Orgs (green fluorescence) towards HSCs (no fluorescence), which could be reduced by Exo^{MSC} (Fig. 5B).

Next, the inflammatory chemokines in the culture supernatants and the fibrosis-related genes of HSCs were collected and analyzed. When Orgs were stimulated alone with IL-17A, the concentration of CXCL10 (mean concentration, Orgs_IL-17A vs. Orgs_Ctrl: 74.6 pg/ml vs. 63.02 pg/ml) (Fig. 4C), IL-6 (413.7 pg/ml vs. 94.52 pg/ml) and CCL20 (1377 pg/ml vs. 103.8 pg/ml) (Fig. 5C) increased significantly relative to the Ctrl group. When the HSCs and Orgs were

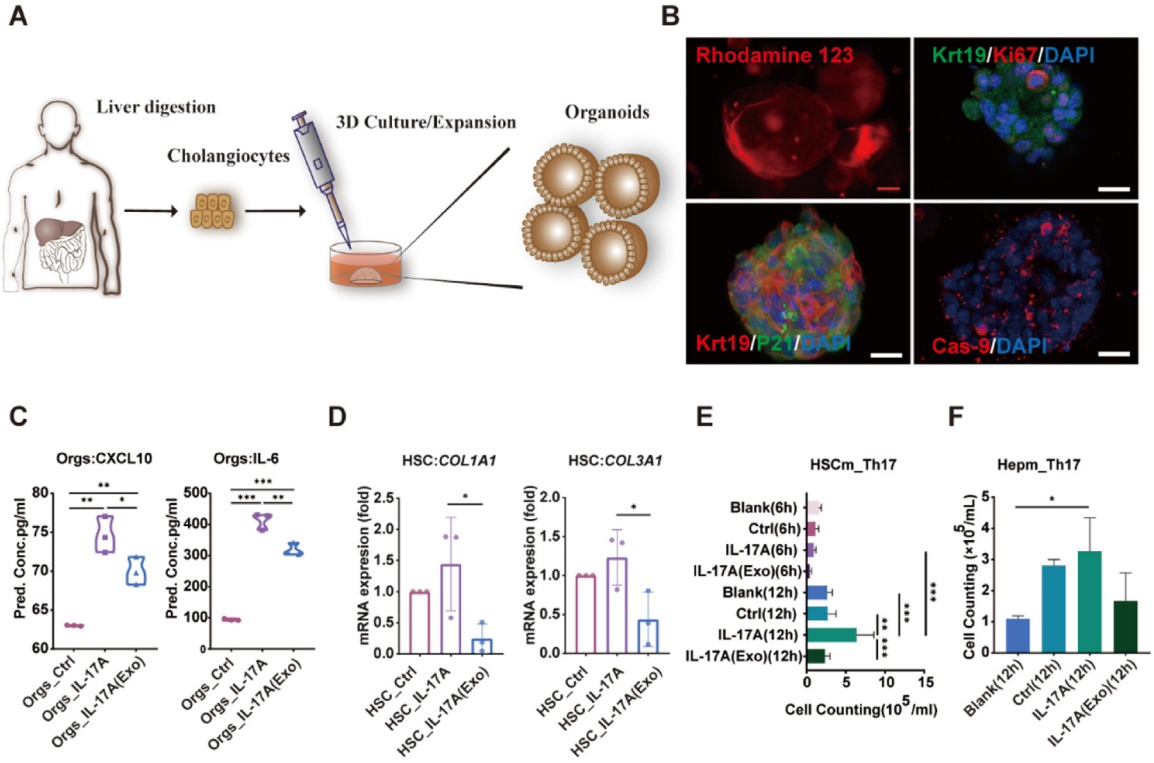

Fig. 4 – Exo^{MSC} moderated the microenvironment associated with Th17-induced fibrosis. (A) Pattern diagram of PSC patient-derived intrahepatic cholangiocytes cultured into Orgs. (B) Identification and functional determination of Orgs by IF analysis. Bile duct marker: Krt19 (red); functional transport activities staining: Rhodamine 123 (red); cell cycle functional proteins: proliferation (Ki67, red), senescence (P21, green), and apoptosis (Cas-9, red). (C) The concentration of CXCL10 and IL-6 in the cultural supernatant of Orgs treated with 100 ng/ml of IL-17A with/without 10 ng/ml of Exo^{MSC} (Orgs_IL-17A(Exo)/Orgs_IL-17A) for 48 h. (D) HSCs cultured with 50 ng/ml of IL-17A with/without 5 ng/ml of Exo^{MSC} (HSC_IL-17A / HSC_IL-17A_(Exo)) for 12 h, with medium only as Ctrl (HSC_Ctrl). The gene expression levels of *COL1A1* and *COL3A1* were determined by qRT-PCR. (E) Cell numbers (/ml) of Th17 (upper chamber) migrating into the supernatant of IL-17A (and Exo^{MSC}) treated HSCs (lower chamber). Th17 cells were counted after 6 h and 12 h. (F) Results of chemotaxis of Th17 response to hepatocyte medium under the same conditions as HSCs. Above all $n = 3–4$.

cultured together in a trans-well (Orgs-H), the paracrine interaction between them promoted a further increase in the expression of inflammatory chemokines such as IL-6 (mean concentration: Orgs_IL-17A vs. Orgs-H_IL-17A: 413.7 pg/ml vs. 8916 pg/ml), IL-1β (0.6825 pg/ml vs. 4.113 pg/ml) and CCL20 (1377 pg/ml vs. 2090 pg/ml) (Fig. 5C). However, the treatment of Exo^{MSC} resulted in a meaningful decrease in the cytokines described above (IL-6, IL-1β, and CCL20), especially the relatively downregulated level of IL-6 ($P < 0.01$) in the Orgs supernatant and CCL20 ($P < 0.01$) in the Orgs-H supernatant. The reduction of CCL20 suggests that Exo^{MSC} attenuated Th17 chemotaxis in the IL-17A-stimulated microenvironment of Orgs-H. Moreover, the expression of *COL3A1* ($P < 0.05$), *COL1A1*, and *vascular cell adhesion molecule 1*(*VCAM1*) showed an increasing trend of fibrosis of Orgs-H induced by IL-17A, and was relatively decreased by Exo^{MSC}. In addition, with IL-17A induction, *COL3A1* expression in HSCs of Orgs-H demonstrated higher compared to HSCs cultured alone (Fig. 4D and 5D).

The above results proved that paracrine interaction between HSCs and cholangiocytes enhanced the hypersecretory phenotype of cholangiocytes and the expression of fibrosis-associated genes of HSCs under IL-17A induction, and Exo^{MSC} could improve this microenvironment.

3.7. *Exo^{MSC} exerted therapeutic effects through the PERK/CHOP pathway and influenced Th17 differentiation via IκBζ regulation*

RNAseq analysis of the livers revealed the differential genes between Mdr2$^{-/-}$ mice and Mdr2$^{-/-}$-Exo mice (Fig. 6A), which were rich in protein processing in the endoplasmic reticulum, P53 signaling pathway, FoxO signaling pathway, tyrosine kinase inhibitor resistance (EGFR), apoptosis, etc., via KEGG pathway enrichment analysis (Fig. 6B). The relevant differential genes of the top 5 signal pathways are listed at Fig. 6C, indicating the downregulating effect of Exo^{MSC} in Mdr2$^{-/-}$ mice. The expression of differential genes (Fig. 6D)

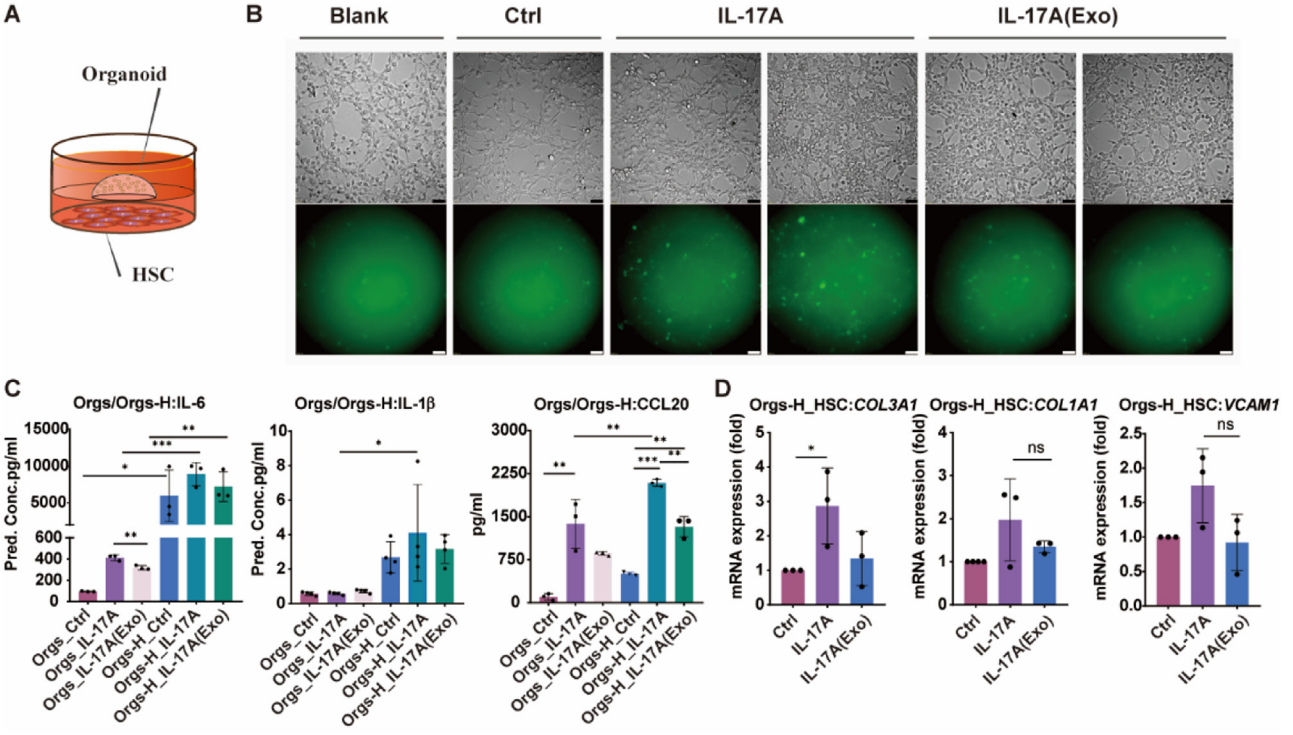

Fig. 5 – Exo^{MSC} attenuated Th17-induced fibrosis by regulating the HSC-cholangiocyte microenvironment. (A) Trans-well culture model of Orgs (top) and HSC (bottom) (Orgs-H). (B) Trans-well culture of PKH67-stained Orgs (top) and HSCs (bottom) for 48 h, and the secretory vesicle of Orgs endocytosing into HSCs was observed in green fluoresce. First row: HSCs captured under a light microscope (scale bar = 50 μm); second row: HSCs observed under an IF microscope (scale bar = 50 μm). (C) The culture supernatant of Orgs-H was analyzed for the levels of cytokines/chemokines such as IL-6, IL-1β, and CCL20 (n = 3–4). (D) Genes of HSCs were harvested after a trans-well culture of HSCs and Orgs (Orgs-H) for 48 h, and the expression levels of *COL3A1*, *COL1A1*, and *VCAM1* were analyzed by qRT-PCR (n = 3). $P < 0.05$, **$P < 0.01$, ***$P < 0.001$).

and protein markers (Fig. 6E) were then verified through real-time reverse transcription-polymerase chain reaction (RT-PCR) and WB analyses. Apoptosis-related genes, such as *Bcl-xl*, *Ask1*, *Bim*, and *Timp*, were higher in Mdr2$^{-/-}$ mice and reduced significantly by Exo^{MSC}. However, the protein marker verification results matched better with the protein processing endoplasmic reticulum pathway (protein kinase R-like endoplasmic reticulum kinase (PERK), transcription factor 4 (ATF4), and apoptosis-promoting transcription factor C/EBP homologous protein (CHOP), etc.), the former phase of apoptosis pathway, as validated by WB (Fig. 6E) that the expression of PERK, CHOP, and ATF4 (upper ladder) were clearly reduced in the exosome-treated groups.

What's more, the phosphorylation of eukaryotic initiation factor-2α (p-eIF2α) was found down-regulated in livers (Fig. 6E). Previous research provides the relationship of p-eIF2α and the protein expression of IκBζ in Th17 differentiation, therefore, we were curious about whether the downregulation effect of p-eIF2α would influence the Th17 differentiation-related essential transfer factors IκBζ [69]. As shown in Fig. 6F, we found that p-eIF2α was downregulated in an exosome concentration-dependent manner during Th17 differentiation, and the expression of IκBζ was gradually downregulated with increasing exosome concentration. Meanwhile, the expression of signal transducer and activator of transcription 3 (Stat3), another transactor closely related to IκBζ, was increased in an exosome concentration-dependent manner, suggesting that Stat3 expression may be affected by Exo^{MSC}. Together, these findings demonstrate the role of p-eIF2α/IκBζ in Th17 differentiation and the important effect of Exo^{MSC} on Th17 persistence.

3.8. *Construction of multicellular organoid systems and validation of the PERK/CHOP pathway*

Our previous work demonstrated that exosomes can regulate the PERK/CHOP pathway to cure Mdr2$^{-/-}$ mice, but whether this signal pathway functions in the Th17-induced microenvironment remains unknown. Therefore, the protein expression of PERK, CHOP, and ATF4 was examined by WB in a trans-well model of co-culture Orgs with hepatocytes or HSCs, but the results presented were not as expected (Fig. S4). This may be due to the inability of trans-well cell cultured systems to efficiently mimic the complex in vivo microenvironment, whereupon multicellular organoids were established to recapitulate the cell-cell connection and demonstrate the more elaborate regulation of signaling pathways in the IL-17A-induced microenvironment.

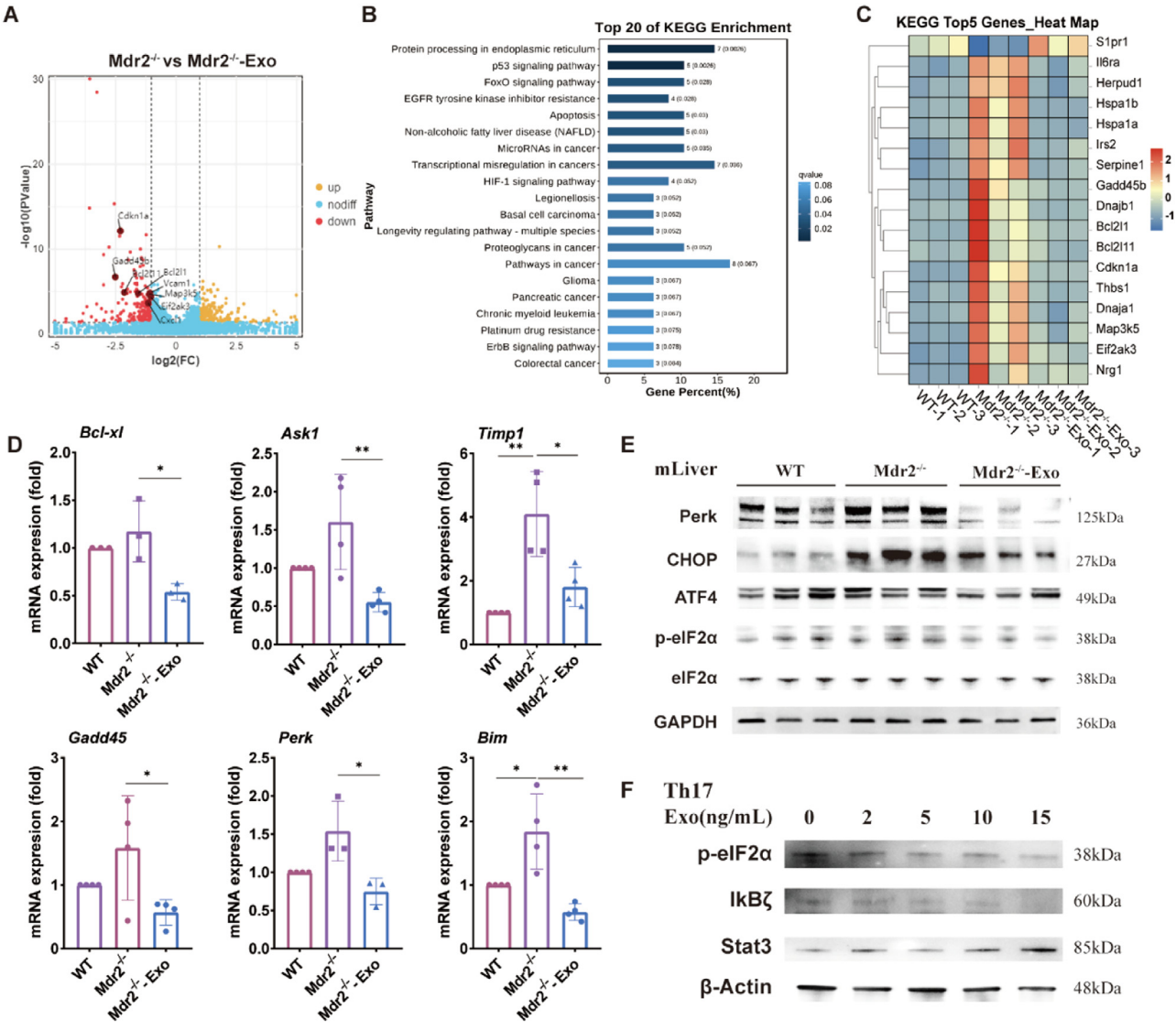

Fig. 6 – Exo^{MSC} exerted therapeutic effects through the PERK/p-Eif2α/CHOP pathway and influenced Th17 differentiation via IκBζ downregulation. (A) Mouse liver RNA-Seq results: differentiation genes between Mdr2$^{-/-}$ and Mdr2$^{-/-}$-Exo mice presented in a volcano map. (B) Bar graph of the top 20 of KEGG enrichment signal pathways analyzed from the differential genes between Mdr2$^{-/-}$ mice and Mdr2$^{-/-}$-Exo mice. (C) Detailed differential genes in the top 5 KEGG pathways listed as a heat map. (D) Typical differential genes were verified by qRT-PCR (n = 3–4, mean ± SD). (E) Mouse liver proteins were extracted and detected; the expression of the pathway markers was verified by WB analysis. (n = 3). (F) The protein of Th17 cells differentiated in vitro (treated with Exo^{MSC}) was harvested and analyzed by WB.

Fig. 7A shows the procedure of the 3D co-culture pattern of cholangiocytes and HSC/hepatocytes (HSC-orgs/Hep-orgs). Fluorescence imaging shows that Hep-orgs are composed of a Krt19^{+} cholangiocyte sphere surrounded by Alb^{+} hepatocytes (Fig. 7B). The hepatocyte subsets aggregated near the Hep-orgs (Fig. 7B, arrow), but α-SMA^{+} HSCs are seen adhering to the cholangiocyte layer from the periphery of the Krt19^{+} cholangiocyte spheres (Fig. 7C) and insert into the intercellular space between cholangiocytes (Fig. 7C, arrow), which corresponds to the anatomical localization of hepatocytes/HSCs and cholangiocytes in the liver tissue (Fig. 7D).

Then, questions were raised as to whether these multicellular organoid systems could simulate the in vivo environment and serve as a better model for mechanistic studies. IF analysis showed that the distribution of PERK was clustered around the nucleus, whereas CHOP was presented in the cytoplasm of Hep-orgs, but this was reversed in HSC-orgs, which may be due to the different anatomical localization of hepatocytes and HSCs in the 3D spheroid (Fig. 7E and 7G). To quantify the protein expression levels, IHC staining was performed and analyzed using Image-Pro-Plus (Fig. 7F and 7H). PERK was found to be upregulated after IL-17A simulation in Hep-orgs ($P < 0.05$) and HSC-orgs ($P < 0.001$) compared

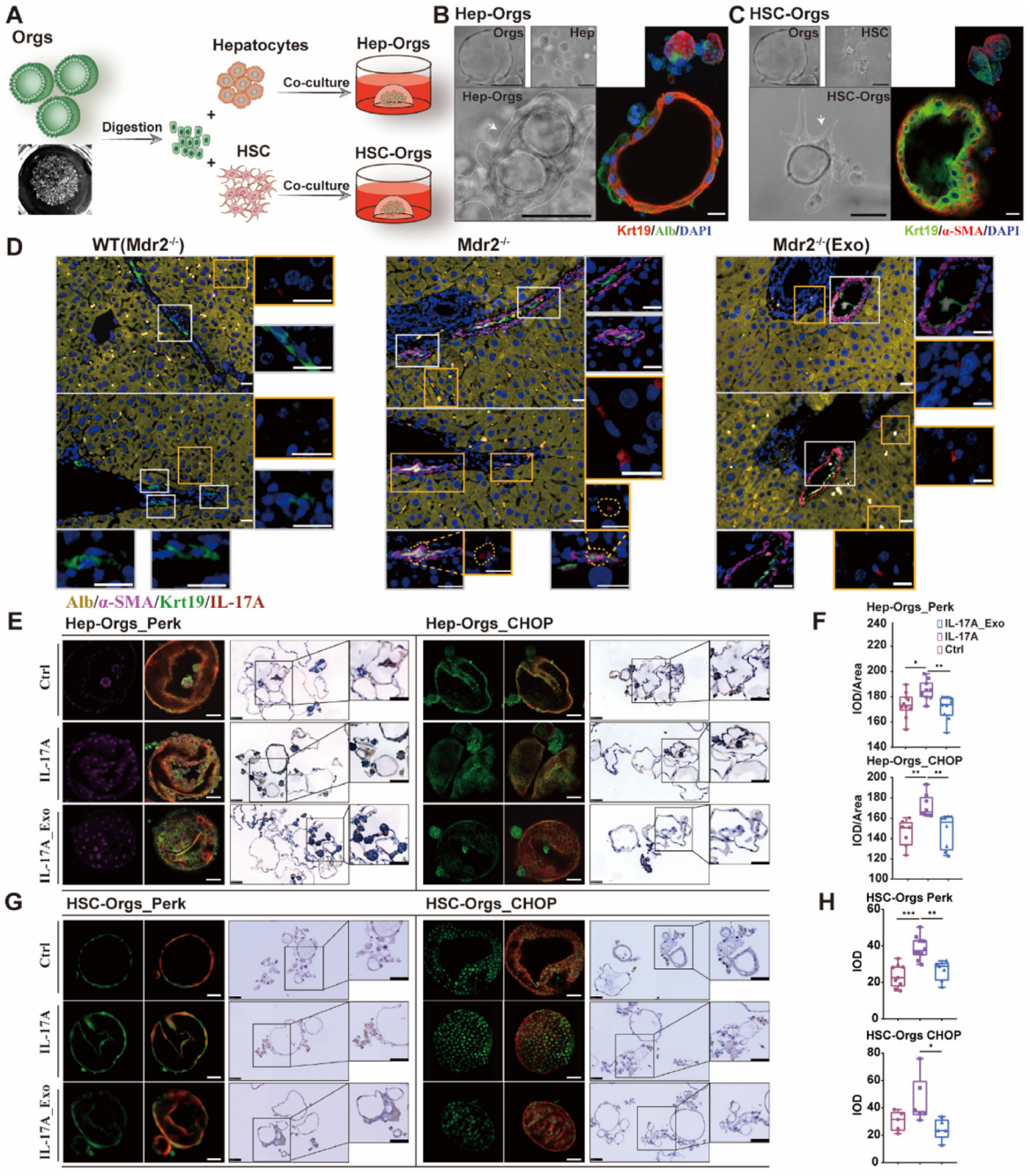

Fig. 7 – Establishment of multicellular organoid systems and verification of the PERK/CHOP pathway. (A) The culture process of multicellular Orgs. (B) Identification of Hep-orgs. Cells cultured separately (top: Orgs, Hep) or together (bottom: Hep-orgs) in Matrigel. Hep-orgs: Krt19^{+} (red) sphere surrounded by Alb^{+} (green) hepatocytes (scale bar = 50 μm). Arrow: Hepatocyte subsets aggregated near the Hep-orgs. (C) Cholangiocytes and HSCs cultured separately (top: Orgs, HSCs) or together (bottom: HSC-orgs) in Matrigel (scale bar = 50 μm). α-SMA^{+} HSCs (red) were shown inserted into the Krt19^{+} (green) sphere (scale bar = 50 μm). IF graphs were imaged by LSCFM. (D) Mouse liver sections stained for Alb^{+} hepatocytes (yellow), Krt19^{+}cholangiocytes (green), α-SMA^{+} HSCs (pink) and IL-17A^{+} cells (red), with the nucleus stained blue (DAPI). (magnified image: scale bar = 20 μm). (E) Protein distribution and expression of PERK and CHOP in Hep-orgs (Hep-orgs PERK: purple, Krt19: red; Alb: green; Hep-orgs CHOP: green, Krt19: red) and IHC staining (scale bar = 50 μm). (F) A total of 7–10 views of the IHC staining results of PERK and CHOP were randomly selected for analysis using Image-Pro Plus. (G) Identification of PERK and CHOP in HSC-orgs was verified by IF (PERK/CHOP: green; Krt19: red) and IHC staining (scale bar = 50 μm). (H) A total of 56 views of IHC staining results for PERK and 7–10 views for CHOP were randomly selected and analyzed. $P < 0.05$, $^{**}P < 0.01$, $^{***}P < 0.001$).

to the Ctrl group, whereas it was significantly inhibited by Exo^{MSC} (both P <0.01). Similarly, CHOP was more markedly increased in Hep-orgs (P < 0.01) under IL-17A stimulation, whereas it was relatively reduced by Exo^{MSC} in both Hep-orgs (P < 0.01) and HSC-orgs (P < 0.05).

Collectively, these data demonstrated that (1) PERK and CHOP are critical signaling markers as stimulated by IL-17A, which could be downregulated by Exo^{MSC}; (2) hepatocyte/HSC-cholangiocyte interaction is more important in PERK/CHOP signaling, but the detailed mechanism needs to be investigated; (3) multicellular organoid systems are closer to the in vivo microenvironment and facilitate mechanistic studies.

3.9. *Discussion*

Here, we explored the anti-fibrotic role of Exo^{MSC} in a PSC mouse model (Mdr2$^{-/-}$ mice) and organoid cultures derived from PSC patient livers. Typical “onion-skin” type fibrosis was alleviated by Exo^{MSC}, and fibrosis-related genes were downregulated in mouse and in vitro IL-17A-induced microenvironment. MSC-derived exosomes were confirmed to have the ability to target and migrate to the damaged liver, as previously demonstrated [54], and our study provided evidence that the liver microenvironment can also be improved by Exo^{MSC}, as followed a reduction in the chemotaxis of Th17 cell to the portal area combined with decreased secretion of IL-17A; an improvement in the hypersecretory phenotype of cholangiocytes with decreased secretion of inflammatory chemokines; decreased expression of fibrotic genes in HSCs; and an improvement in the interaction between HSCs and cholangiocytes.

The accumulation of unfolded proteins in the endoplasmic reticulum caused the release and activation of message proteins from the luminal stress-sensing domains (PERK) of the unfolded protein response effectors, followed by the phosphorylation of eIF2α at serine-51 [70], consequently reducing the rate of translation initiation. Then, the downstream effector ATF4 and CHOP were increased upon endoplasmic reticulum stress [71]. Evidence was obtained proving that the cholestatic liver fibrosis and inflammatory responses induced by BDL are inhibited in CHOP$^{-/-}$ mice [72], indicating the important role of CHOP in the endoplasmic reticulum (ER) stress-related hepatic fibrosis of BDL mice. In Exo^{MSC}-treated Mdr2$^{-/-}$ mice, we revealed the downregulation of protein processing in the endoplasmic reticulum pathway, as well as the downregulation of the level of PERK by Exo^{MSC}; additionally, a reduction in ATF4 activation could further reduce the expression of CHOP. To further verify the expression and distribution of these two proteins under stimulation with IL-17A, based on the previous culture system [67], we established a multicellular organoid system—HSC-orgs and Hep-orgs, compared to the trans-well culture system, revealing the essential role of direct cellular interaction in signaling pathway transmission. Our multicellular organoid system overcomes the inability of single-cell-derived organoids, instead being closer to the multicellular microenvironmental state of the organs.

Our research found that the p-eIF2α expression in the liver is down-regulated by Exo^{MSC}, while eIF2α remains unchanged, implying that a relative decrease in p-eIF2α may help to alleviate ER stress and thus improve the cellular conditions of the hepatic microenvironment due to the pathological state of IL-17 stimulation. As for the relationship between eIF2α and the differentiation of Th17 cells, Chen et al. verified that the downregulation of p-eIF2α promotes the differentiation of Th17 via IκBζ [69]. However, though the reduction of p-eIF2α in Th17 differentiation progressed in our research, the expression of IκBζ expression remained downregulated by exosomes, as proven by in vitro experiments. Besides, IκBζ was demonstrated directly binding to the regulatory region of the IL-17 gene [73], and IL-17A expression was downregulated after Th17 differentiation was inhibited by Exo^{MSC} in our research. Therefore, we suspect that the direct role of exosomes in Th17 differentiation is even more pronounced for transcription factors, and primarily mediated through the targeted inhibition of IκBζ expression, but the upregulation of Stat3 [34] did not have a persistent effect on the maturation of Th17. Considering that exosomes are rich in miRNAs, proteins, etc., exactly what regulates the expression of IκBζ involved in Th17 will be the subject of our further research.

The latest research showed that circulating naïve T cells in patients with PSC were predisposed to be polarized towards Th17 cells, a population of cells proven to have a transcriptome and T cell receptor-like circulation naïve T cells, but express genes related to tissue residency [2]. In line with this, we also found in PSC mice (Mdr2$^{-/-}$ mice) that IL-17A- expressing cells were distributed more around the fibrotic confluent area, whose differentiation progress in the liver could be inhibited by multiple injections of Exo^{MSC}. In addition, shreds of evidence showed the important role of IκBζ (protein or gene) inhibition in curing refractory diseases, such as imiquimod-induced psoriasis [74] and colorectal cancer [75]. Furthermore, as previously demonstrated, recruited Th17 cells entering the portal tracts [76] could exacerbate the fibrotic microenvironment through positive feedback regulation. Given the critical role of Th17 in PSC fibrosis and the profibrotic role of IL-17A in the liver microenvironment, particularly between HSCs and cholangiocytes found in our study, we revealed that Exo^{MSC} may act as an effective therapeutic tool to alleviate fibrosis by inhibiting Th17 differentiation and reliving ER stress in PSC or other Th17-related diseases.

4. Conclusion

Based on Mdr2$^{-/-}$ mice and the organoids derived from PSC patients, our investigation disclosed that Exo^{MSC} could alleviate liver fibrosis in PSC disease by inhibiting Th17 differentiation through downregulated IκBζ expression, and ameliorate the Th17-induced microenvironment, including improving the hypersecretory phenotype of cholangiocytes and the interaction between HSCs and cholangiocytes by regulating PERK/CHOP signaling, which will be a potential therapy for PSC or Th17-associated diseases. Moreover, multicellular organoids possess the benefits of being in closer proximity to the in vivo microenvironment than the trans-well co-culture system. This implies an immense potential

for preclinical disease modeling and therapeutic mechanism research of the novel multicellular organoids.

Conflicts of interest

The authors declare that they have no known competing financial interests or personal relationships that could have appeared to influence the work reported in this paper.

Acknowledgments

This work was supported by grants for National Key Research and Development Program of China (No. 2020YFA0113003), Key Research and Development Project of Zhejiang Province (No. 2023C03046), Fundamental Research Funds for the Central Universities (No. 2022ZFJH003), and Research Project of Jinan Microecological Biomedicine Shandong Laboratory (No. JNL-2022026C, JNL-2023003C).

Supplementary materials

Supplementary material associated with this article can be found, in the online version, at doi:10.1016/j.ajps.2024.100889.

References

[1] Sato K, Glaser S, Kennedy L, Liangpunsakul S, Meng F, Francis H, et al. Preclinical insights into cholangiopathies: disease modeling and emerging therapeutic targets. Expert Opin Ther Targets 2019;23(6):461–72.
[2] Poch T, Krause J, Casar C, Liwinski T, Glau L, Kaufmann M, et al. Single-cell atlas of hepatic T cells reveals expansion of liver-resident naive-like $CD4^{+}$T cells in primary sclerosing cholangitis. J Hepatol 2021;75(2):414–23.
[3] Eaton JE, Talwalkar JA, Lazaridis KN, Gores GJ, Lindor KD. Pathogenesis of primary sclerosing cholangitis and advances in diagnosis and management. Gastroenterology 2013;145(3):521–36.
[4] Karlsen TH, Folseraas T, Thorburn D, Vesterhus M. Primary sclerosing cholangitis - a comprehensive review. J Hepatol 2017;67(6):1298–323.
[5] Sato K, Zhang W, Safarikia S, Isidan A, Chen AM, Li P, et al. Organoids and spheroids as models for studying cholestatic liver injury and cholangiocarcinoma. Hepatology 2021;74(1):491–502.
[6] Hirschfield GM, Gershwin ME. The Immunobiology and pathophysiology of primary biliary cirrhosis. Ann Rev Pathol: Mech Dis 2013;8:303–30.
[7] Nakamoto N, Sasaki N, Aoki R, Miyamoto K, Suda W, Teratani T, et al. Gut pathobionts underlie intestinal barrier dysfunction and liver T helper 17 cell immune response in primary sclerosing cholangitis. Nat Microbiol 2019;4(3):492–503.
[8] Kummen M, Holm K, Anmarkrud JA, Nygard S, Vesterhus M, Hoivik ML, et al. The gut microbial profile in patients with primary sclerosing cholangitis is distinct from patients with ulcerative colitis without biliary disease and healthy controls. Gut 2017;66(4):611–19.
[9] Lazaridis KN, LaRusso NF. Primary sclerosing cholangitis. New Engl J Med 2016;375(12):1161–70.
[10] Soroka CJ, Assis DN, Alrabadi LS, Roberts S, Cusack L, Jaffe AB, et al. Bile-derived organoids from patients with primary sclerosing cholangitis recapitulate their inflammatory immune profile. Hepatology 2019;70(3):871–82.
[11] Fickert P, Fuchsbichler A, Wagner M, Zollner G, Kaser A, Tilg H, et al. Regurgitation of bile acids from leaky bile ducts causes sclerosing cholangitis in Mdr2 (Abcb4) knockout mice. Gastroenterology 2004;127(1):261–74.
[12] Fickert P, Fuchsbichler A, Marschall HU, Wagner M, Zollner G, Krause R, et al. Lithocholic acid feeding induces segmental bile duct obstruction and destructive cholangitis in mice. Am J Pathol 2006;168(2):410–22.
[13] Nishio T, Hu R, Koyama Y, Liang S, Rosenthal SB, Yamamoto G, et al. Activated hepatic stellate cells and portal fibroblasts contribute to cholestatic liver fibrosis in MDR2 knockout mice. J Hepatol 2019;71(3):573–85.
[14] Miethke AG, Zhang W, Simmons J, Taylor AE, Shi T, Shanmukhappa SK, et al. Pharmacological inhibition of apical sodium-dependent bile acid transporter changes bile composition and blocks progression of sclerosing cholangitis in multidrug resistance 2 knockout mice. Hepatology 2016;63(2):512–23.
[15] Baghdasaryan A, Fuchs CD, Österreicher CH, Lemberger UJ, Halilbasic E, Påhlman I, et al. Inhibition of intestinal bile acid absorption improves cholestatic liver and bile duct injury in a mouse model of sclerosing cholangitis. J Hepatol 2016;64(3):674–81.
[16] Lazaridis KN, Strazzabosco M, Larusso NF. The cholangiopathies: disorders of biliary epithelia. Gastroenterology 2004;127(5):1565–77.
[17] Fickert P, Pollheimer MJ, Beuers U, Lackner C, Hirschfield G, Housset C, et al. Characterization of animal models for primary sclerosing cholangitis (PSC). J Hepatol 2014;60(6):1290–303.
[18] Prior N, Inacio P, Huch M. Liver organoids: from basic research to therapeutic applications. Gut 2019;68(12):2228–37.
[19] Brevini T, Tysoe OC, Sampaziotis F. Tissue engineering of the biliary tract and modelling of cholestatic disorders. J Hepatol 2020;73(4):918–32.
[20] Mischiati C, Ura B, Roncoroni L, Elli L, Cervellati C, Squerzanti M, et al. Changes in protein expression in two cholangiocarcinoma cell lines undergoing formation of multicellular tumor spheroids in vitro. PLoS One 2015;10(3):e0118906.
[21] Lancaster MA, Knoblich JA. Organogenesis in a dish: modeling development and disease using organoid technologies. Science 2014;345(6194):1247125.
[22] Ouchi R, Togo S, Kimura M, Shinozawa T, Koido M, Koike H, et al. Modeling steatohepatitis in humans with pluripotent stem cell-derived organoids. Cell Metab 2019;30(2):374–84 e6.
[23] Tsai S, McOlash L, Palen K, Johnson B, Duris C, Yang Q, et al. Development of primary human pancreatic cancer organoids, matched stromal and immune cells and 3D tumor microenvironment models. BMC Cancer 2018;18(1):335.
[24] Kim M, Mun H, Sung CO, Cho EJ, Jeon HJ, Chun SM, et al. Patient-derived lung cancer organoids as in vitro cancer models for therapeutic screening. Nat Commun 2019;10(1):3991.
[25] Jager M, Blokzijl F, Sasselli V, Boymans S, Janssen R, Besselink N, et al. Measuring mutation accumulation in single human adult stem cells by whole-genome sequencing of organoid cultures. Nat Protoc 2018;13(1):59–78.
[26] Kimura M, Iguchi T, Iwasawa K, Dunn A, Thompson WL, Yoneyama Y, et al. En masse organoid phenotyping informs metabolic-associated genetic susceptibility to NASH. Cell 2022;185(22):4216–32 e16.
[27] Vesterhus M, Holm A, Hov JR, Nygård S, Schrumpf E, Melum E, et al. Novel serum and bile protein markers predict

primary sclerosing cholangitis disease severity and prognosis. J Hepatol 2017;66(6):1214–22.
[28] Zweers SJ, Shiryaev A, Komuta M, Vesterhus M, Hov JR, Perugorria MJ, et al. Elevated interleukin-8 in bile of patients with primary sclerosing cholangitis. Liver Int 2016;36(9):1370–7.
[29] Strazzabosco M, Fiorotto R, Cadamuro M, Spirli C, Mariotti V, Kaffe E, et al. Pathophysiologic implications of innate immunity and autoinflammation in the biliary epithelium. Biochim Biophys Acta Mol Basis Dis 2018;1864(4 Pt B): 1374–1379.
[30] Wu N, Meng F, Zhou T, Venter J, Giang TK, Kyritsi K, et al. The secretin/secretin receptor axis modulates ductular reaction and liver fibrosis through changes in transforming growth factor-β1-mediated biliary senescence. Am J Pathol 2018;188(10):2264–80.
[31] Oo YH, Banz V, Kavanagh D, Liaskou E, Withers DR, Humphreys E, et al. CXCR3-dependent recruitment and CCR6-mediated positioning of Th-17 cells in the inflamed liver. J Hepatol 2012;57(5):1044–51.
[32] Hang S, Paik D, Yao L, Kim E, Trinath J, Lu J, et al. Bile acid metabolites control T(H)17 and T(reg) cell differentiation. Nature 2019;576(7785):143–8.
[33] Su Y, Lu N, Li Q, Wen H, Zhang XQ, Zhang M. Gut Microbiota and drug-related liver injury: challenges and perspectives. Adv Gut Microbiome Res 2023;2023:5442597.
[34] Meng F, Wang K, Aoyama T, Grivennikov SI, Paik Y, Scholten D, et al. Interleukin-17 signaling in inflammatory, Kupffer cells, and hepatic stellate cells exacerbates liver fibrosis in mice. Gastroenterology 2012;143(3):765–76 e3.
[35] Berardis S, Dwisthi Sattwika P, Najimi M, Sokal EM. Use of mesenchymal stem cells to treat liver fibrosis: current situation and future prospects. World J Gastroenterol 2015;21(3):742–58.
[36] Ge J, Wang K, Meng QH, Qi ZX, Meng FL, Fan YC. Implication of Th17 and Th1 cells in patients with chronic active hepatitis B. J Clin Immunol 2010;30(1):60–7.
[37] Lemmers A, Moreno C, Gustot T, Maréchal R, Degré D, Demetter P, et al. The interleukin-17 pathway is involved in human alcoholic liver disease. Hepatology 2009;49(2):646–657.
[38] Sato K, Kennedy L, Liangpunsakul S, Kusumanchi P, Yang Z, Meng F, et al. Intercellular communication between hepatic cells in liver diseases. Int J Mol Sci 2019;20(9):2180.
[39] Bataller R, Brenner DA. Liver fibrosis. J Clin Invest 2005;115(2):209–18.
[40] Iwaisako K, Jiang C, Zhang M, Cong M, Moore-Morris TJ, Park TJ, et al. Origin of myofibroblasts in the fibrotic liver in mice. Proc Natl Acad Sci USA 2014;111(32):E3297–305.
[41] Kisseleva T, Uchinami H, Feirt N, Quintana-Bustamante O, Segovia JC, Schwabe RF, et al. Bone marrow-derived fibrocytes participate in pathogenesis of liver fibrosis. J Hepatol 2006;45(3):429–38.
[42] Wells RG, Schwabe RF. Origin and function of myofibroblasts in the liver. Semin Liver Dis 2015;35(2):97–106.
[43] Friedman SL, Roll FJ, Boyles J, Bissell DM. Hepatic lipocytes: the principal collagen-producing cells of normal rat liver. Proc Natl Acad Sci USA 1985;82(24):8681–5.
[44] Seki E, De Minicis S, Osterreicher CH, Kluwe J, Osawa Y, Brenner DA, et al. TLR4 enhances TGF-beta signaling and hepatic fibrosis. Nat Med 2007;13(11):1324–32.
[45] Sato K, Marzioni M, Meng F, Francis H, Glaser S, Alpini G. Ductular reaction in liver diseases: pathological mechanisms and translational significances. Hepatology 2019;69(1):420–30.
[46] Di Nicola M, Carlo-Stella C, Magni M, Milanesi M, Longoni PD, Matteucci P, et al. Human bone marrow stromal cells suppress T-lymphocyte proliferation induced by cellular or nonspecific mitogenic stimuli. Blood 2002;99(10):3838–43.
[47] Bartholomew A, Sturgeon C, Siatskas M, Ferrer K, McIntosh K, Patil S, et al. Mesenchymal stem cells suppress lymphocyte proliferation in vitro and prolong skin graft survival in vivo. Exp Hematol 2002;30(1):42–8.
[48] Augello A, Tasso R, Negrini SM, Amateis A, Indiveri F, Cancedda R, et al. Bone marrow mesenchymal progenitor cells inhibit lymphocyte proliferation by activation of the programmed death 1 pathway. Eur J Immunol 2005;35(5):1482–90.
[49] Pianta S, Bonassi Signoroni P, Muradore I, Rodrigues MF, Rossi D, Silini A, et al. Amniotic membrane mesenchymal cells-derived factors skew T cell polarization toward Treg and downregulate Th1 and Th17 cells subsets. Stem Cell Rev Rep 2015;11(3):394–407.
[50] Le Blanc K, Mougiakakos D. Multipotent mesenchymal stromal cells and the innate immune system. Nat Rev Immunol 2012;12(5):383–96 Epub 2012/04/26.
[51] Kalluri R, LeBleu VS. The biology, function, and biomedical applications of exosomes. Science 2020;367(6478):eaau6977.
[52] Psaraki A, Ntari L, Karakostas C, Korrou-Karava D, Roubelakis MG. Extracellular vesicles derived from mesenchymal stem/stromal cells: the regenerative impact in liver diseases. Hepatology 2022;75(6):1590–603.
[53] Kordelas L, Rebmann V, Ludwig AK, Radtke S, Ruesing J, Doeppner TR, et al. MSC-derived exosomes: a novel tool to treat therapy-refractory graft-versus-host disease. Leukemia 2014;28(4):970–3.
[54] Lin F, Chen W, Zhou J, Zhu J, Yao Q, Feng B, et al. Mesenchymal stem cells protect against ferroptosis via exosome-mediated stabilization of SLC7A11 in acute liver injury. Cell Death Dis 2022;13(3):271.
[55] Qu Y, Zhang Q, Cai X, Li F, Ma Z, Xu M, et al. Exosomes derived from miR-181-5p-modified adipose-derived mesenchymal stem cells prevent liver fibrosis via autophagy activation. J Cell Mol Med 2017;21(10):2491–502.
[56] Lou G, Yang Y, Liu F, Ye B, Chen Z, Zheng M, et al. MiR-122 modification enhances the therapeutic efficacy of adipose tissue-derived mesenchymal stem cells against liver fibrosis. J Cell Mol Med 2017;21(11):2963–73.
[57] Lou G, Chen Z, Zheng M, Liu Y. Mesenchymal stem cell-derived exosomes as a new therapeutic strategy for liver diseases. Exp Mol Med 2017;49(6):e346.
[58] Li T, Yan Y, Wang B, Qian H, Zhang X, Shen L, et al. Exosomes derived from human umbilical cord mesenchymal stem cells alleviate liver fibrosis. Stem Cells Dev 2013;22(6):845–54.
[59] Chen L, Lu FB, Chen DZ, Wu JL, Hu ED, Xu LM, et al. BMSCs-derived miR-223-containing exosomes contribute to liver protection in experimental autoimmune hepatitis. Mol Immunol 2018;93:38–46.
[60] Li J, Ghazwani M, Zhang Y, Lu J, Li J, Fan J, et al. miR-122 regulates collagen production via targeting hepatic stellate cells and suppressing P4HA1 expression. J Hepatol 2013;58(3):522–8.
[61] Yang JJ, Liu LP, Tao H, Hu W, Shi P, Deng ZY, et al. MeCP2 silencing of LncRNA H19 controls hepatic stellate cell proliferation by targeting IGF1R. Toxicology 2016;359-360:39–46.
[62] Hyun J, Wang S, Kim J, Kim GJ, Jung Y. MicroRNA125b-mediated Hedgehog signaling influences liver regeneration by chorionic plate-derived mesenchymal stem cells. Sci Rep 2015;5:14135.
[63] Chen W, Zhu J, Lin F, Xu Y, Feng B, Feng X, et al. Human placenta mesenchymal stem cell-derived exosomes delay H_2O_2-induced aging in mouse cholangioids. Stem Cell Res Ther 2021;12(1):201.
[64] Yao Q, Chen W, Yu Y, Gao F, Zhou J, Wu J, et al. Human placental mesenchymal stem cells relieve primary sclerosing cholangitis via upregulation of TGR5 in Mdr2(-/-) Mice

and human intrahepatic cholangiocyte organoid models. Research 2023;6:0207.
[65] Niknam B, Baghaei K, Mahmoud Hashemi S, Hatami B, Reza Zali M, Amani D. Human Wharton's jelly mesenchymal stem cells derived-exosomes enriched by miR-124 promote an anti-fibrotic response in an experimental model of liver fibrosis. Int Immunopharmacol 2023;119:110294.
[66] Lin Y, Yan M, Bai Z, Xie Y, Ren L, Wei J, et al. Huc-MSC-derived exosomes modified with the targeting peptide of aHSCs for liver fibrosis therapy. J Nanobiotechnology 2022;20(1):432.
[67] Chen W, Yao Q, Wang R, Fen B, Chen J, Xu Y, et al. Highly efficient methods to culture mouse cholangiocytes and small intestine organoids. Front Microbiol 2022;13:907901.
[68] Stein S, Henze L, Poch T, Carambia A, Krech T, Preti M, et al. IL-17A/F enable cholangiocytes to restrict T cell-driven experimental cholangitis by upregulating PD-L1 expression. J Hepatol 2021;74(4):919–30.
[69] Chen L, Bai J, Peng D, Gao Y, Cai X, Zhang J, et al. SZB120 exhibits immunomodulatory effects by targeting eIF2α to suppress Th17 cell differentiation. J Immunol 2021;206(5):953–62.
[70] Marciniak SJ, Garcia-Bonilla L, Hu J, Harding HP, Ron D. Activation-dependent substrate recruitment by the eukaryotic translation initiation factor 2 kinase PERK. J Cell Biol 2006;172(2):201–9.
[71] Atkins C, Liu Q, Minthorn E, Zhang SY, Figueroa DJ, Moss K, et al. Characterization of a novel PERK kinase inhibitor with antitumor and antiangiogenic activity. Cancer Res 2013;73(6):1993–2002.
[72] Liu R, Li X, Huang Z, Zhao D, Ganesh BS, Lai G, et al. C/EBP homologous protein-induced loss of intestinal epithelial stemness contributes to bile duct ligation-induced cholestatic liver injury in mice. Hepatology 2018;67(4):1441–57.
[73] Dong C. Genetic controls of Th17 cell differentiation and plasticity. Exp Mol Med 2011;43(1):1–6.
[74] Mandal A, Kumbhojkar N, Reilly C, Dharamdasani V, Ukidve A, Ingber DE, et al. Treatment of psoriasis with NFKBIZ siRNA using topical ionic liquid formulations. Sci Adv 2020;6(30):eabb6049.
[75] Kakiuchi N, Yoshida K, Uchino M, Kihara T, Akaki K, Inoue Y, et al. Frequent mutations that converge on the NFKBIZ pathway in ulcerative colitis. Nature 2020;577(7789):260–5.
[76] Kunzmann LK, Schoknecht T, Poch T, Henze L, Stein S, Kriz M, et al. Monocytes as potential mediators of pathogen-induced T-helper 17 differentiation in patients with primary sclerosing cholangitis (PSC). Hepatology 2020;72(4):1310–26.